Anisotropic Multiband Many-Body Interactions in $LuNi_2B_2C$

B. Bergk,[1] V. Petzold,[2,*] H. Rosner,[2] S.-L. Drechsler,[3] M. Bartkowiak,[1] O. Ignatchik,[1] A. D. Bianchi,[1,†] I. Sheikin,[4] P. C. Canfield,[5] and J. Wosnitza[1]

[1]*Hochfeld-Magnetlabor Dresden (HLD), Forschungszentrum Dresden-Rossendorf, D-01314 Dresden, Germany*
[2]*Max-Planck-Institut für Chemische Physik fester Stoffe, D-01187 Dresden, Germany*
[3]*Leibniz-Institute for Solid State and Materials Research (IFW-Dresden), D-01171 Dresden, Germany*
[4]*Grenoble High Magnetic Field Laboratory, CNRS, BP 166, F-38042 Grenoble Cedex 09, France*
[5]*Ames Laboratory and Department of Physics and Astronomy, Iowa State University, Ames, Iowa 50011, USA*

(Received 1 February 2008; published 27 June 2008)

We present a comprehensive de Haas–van Alphen study on the nonmagnetic borocarbide superconductor $LuNi_2B_2C$. The analysis of the angular-dependent effective masses for different bands in combination with full-potential density functional calculations allowed us to determine the mass-enhancement factors, λ, for the different electronic bands and their wave-vector dependences. Our data clearly show the anisotropic multiband character of the superconductivity in $LuNi_2B_2C$.

DOI: 10.1103/PhysRevLett.100.257004 PACS numbers: 74.70.Dd, 71.18.+y, 74.25.Jb

Electron-electron (e-e) and electron-phonon (e-ph) interactions—present in any solid—are the fundamental sources of a rich variety of many-body effects. These effects emerge with (i) the appearance of new broken-symmetry ordered phases or (ii) as renormalization effects in the normal state described for metallic systems in terms of a Fermi liquid. Superconductivity, bond order, charge and spin-density waves, or other magnetic phases are well-known examples for such orderings. The mass renormalization, seen, e.g., in the Sommerfeld coefficient of the electronic specific heat as well as in the de Haas–van Alphen (dHvA) band masses stands for the second type. In the well-studied relation between e-ph interaction and superconductivity, the critical temperature T_c and other superconducting properties are governed by similar coupling constants λ_i, as well as the renormalization of normal-state properties as mentioned above, though they differ in the details of the averaging procedure over some electronic subspaces such as Fermi-surface (FS) sheets, orbits, etc. [1]. The smaller this subspace, the more detailed insight in the microscopic origin of observed anisotropies can be gained. In this context, the analysis of the enhanced dHvA masses [combined with a band-structure calculation based on density functional theory (DFT) to model the corresponding ''bare'' masses] is a unique ''bulk'' technique. It allows for a separate determination of the angular-resolved coupling strength for each observable FS. This information is of large interest, e.g., for the separation of multiband and anisotropic single-band effects in determining superconducting gaps.

The isotropic, effective single-band, strong-coupling Eliashberg theory covers quantitatively most basic properties of many elemental superconductors in assuming an isotropic boson(phonon)-mediated Cooper-pair coupling. For a deeper understanding of more complex type-II superconductors near the clean limit with many atoms per unit cell, though, a better knowledge of the band-resolved strength and anisotropy of the e-ph coupling is a prerequisite. Recently, for MgB_2, such an approach has been performed. It yields different, though isotropic, coupling constants in four well-resolved FSs which can be projected onto two effective FSs [2]. The simple band structure of MgB_2 makes such analysis rather straightforward. The angular and band-resolved determination of the coupling strengths in more complex materials such as $LuNi_2B_2C$ with more involved FSs demands considerable efforts combining experiment and theory.

Here, we apply dHvA measurements combined with highly-precise full-potential local-orbital (FPLO) calculations [3] to the most strongly coupled but still stable borocarbide superconductor $LuNi_2B_2C$ to determine its many-body mass enhancements independently for several bands and for different directions. Experimentally, the effective masses are obtained from the T-dependent dHvA signals. The involved coupling strength, most likely mainly due to e-ph coupling [4], is then extracted from a comparison with the bare masses calculated within a DFT code which does not include such many-body effects. A similar attempt has previously been used for niobium [5]. At that time, however, for this simple cubic system with only one atom per unit cell and less distinct multiband and anisotropy effects, the calculations could not be performed with the present full-potential accuracy. Only now with the achieved progress both in experiment and theory, studies of elaborated materials with a rather involved band structure are possible.

$LuNi_2B_2C$ belongs to the rare-earth transition-metal borocarbide superconductors [6]. These materials display relatively high T_c values up to 23 K. The coexistence of magnetism and superconductivity in many magnetic members of this family attracted considerable attention. Despite numerous studies, some details of the superconductivity are still unclear and, therefore, a matter of interest and debate. Originally, the borocarbides have been considered

as simple phonon-mediated s-wave superconductors [7,8]. Subsequent thermodynamic measurements, however, have led to different suggestions, such as anisotropic s or d-wave [9,10], or $s+g$-wave pairing [11,12]. Finally, caused by the rather elaborate FS with open and closed sheets [13–16], also multiband behavior was suggested [17–22]. It is, therefore, highly desirable to gain more insight into the strength and anisotropy of the coupling in the different bands. This may be helpful to elucidate which bands are mainly involved in the superconductivity and may give a clue about the pairing nature.

The dHvA oscillations on high-quality flux-grown platelet-shaped single crystals of $LuNi_2B_2C$ [23] (onset $T_c = 16.5$ K) were measured by use of a capacitive cantilever torquemeter. The samples were placed on a rotatable platform and were measured in various High Magnetic Field Laboratories in magnetic fields up to 15 T in a superconducting magnet at the HLD in Dresden, up to 28 T in Grenoble, and up to 32 T in Nijmegen. A dilution refrigerator as well as ^{3}He cryostats have been used to cover the T range from 20 mK up to 10 K.

To calculate band structure, FS, and dHvA frequencies of $LuNi_2B_2C$, we applied the FPLO code (version 5.00–18) [3] in its scalar-relativistic version within the local-density approximation. For the exchange and correlation potential, the Perdew-Wang form [24] was used. We used the structural data of Ref. [25]. Lu($4f$, $5s$, $5p$, $5d$, $6s$, $6p$), Ni($3s$, $3p$, $3d$, $4s$, $4p$), B, and C($2s$, $2p$, $3d$) orbitals were chosen as the basis set. Self consistency was obtained using a mesh of 1470 irreducible k-points. The theoretical dHvA data were calculated on an at least 10 times denser k mesh. The band masses for the FS orbits were calculated from the derivative of the corresponding dHvA frequencies with respect to the energy. The calculated band structure close to the Fermi level and the corresponding FSs are presented in Fig. 1.

Figure 2 shows the angular dependence of all observed dHvA frequencies for the main crystallographic directions. The predicted DFT frequencies (solid lines) are also included. Our dHvA data agree well with a previous result reported only for one crystal orientation of $LuNi_2B_2C$ [26]. The overall angular dependence of the dHvA data resembles that of the better studied isostructural system YNi_2B_2C [27–29]. Some distinctions are, however, found especially around the [001] axis.

By comparing the calculated FSs (Figs. 1 and 2) with the data, we can assign the observed dHvA frequencies to certain bands. For the cubic and the "cushion"-like FSs, the calculations and the measured data are perfectly in line, only for the spheroidal (red) FS deviations are found. More experimental data for this sample are given in Ref. [30]. The oscillations with frequency F_α are very pronounced in the spectrum. Because of the low effective mass, these oscillations were unambiguously determined in all crystallographic orientations. The observed angular dependence has a spheroidal shape and agrees with the DFT prediction which is, however, shifted by about 400 T. What looks like a sizable deviation on first glance can be explained by the very small contribution of less then 1% of this FS to the total DOS(ε_F). A tiny shift of the corresponding band filling as low as $0.012e^-$ would bring this FS to excellent agreement with the dHvA data, whereas the change of the dHvA frequencies for the other FS sheets would be negligible. In addition to its small DOS, this FS yields the smallest mass renormalization (see Fig. 3) and is therefore of minor relevance for the superconductivity in $LuNi_2B_2C$.

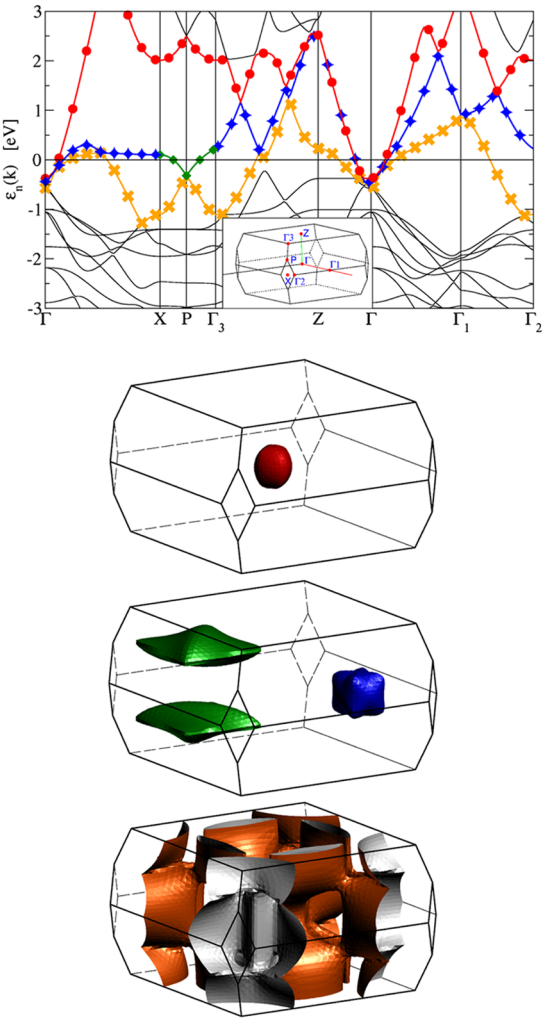

FIG. 1 (color online). Band structure (upper panel) and FSs of $LuNi_2B_2C$. The bands are labeled according to different FSs: circle (red)—ball, diamond (blue)—cube, triangle (green)—cushion, cross (orange)—branched FS. The FS in the third panel was shifted by $(\pi/a, \pi/a, 0)$ to present simply connected sheets.

Our FPLO calculations allow also to identify parts of the complicated branched FS; i.e., around [001], the data at about 12 500 T (Fig. 2) belong to a "lemon"-like extremal orbit, while those at about 2400 T belong to a "windmill"-shaped part of the FS. There are further dHvA frequencies that cannot be assigned directly to a DFT FS. They originate most likely from a splitting or corrugations of some FSs. Such topological modifications of the "ball"-like and cubic FSs would explain most of the unassigned data (open

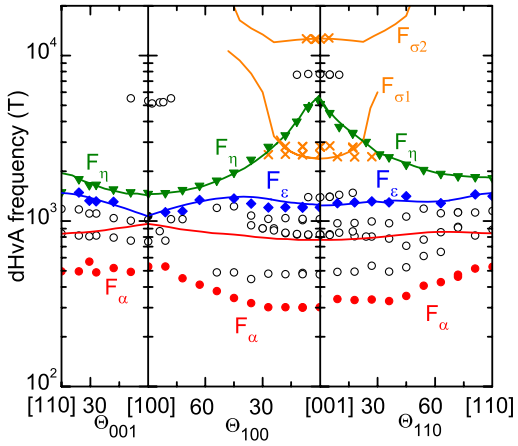

FIG. 2 (color online). Angular dependence of the dHvA frequencies. The solid lines are obtained by use of FPLO calculations. The calculated dHvA frequency for the spherical FS, F_α, is somewhat larger than measured. For the cubic, F_ϵ, the cushion-like, F_η, and the "branched" FSs, $F_{\sigma 1}$ and $F_{\sigma 2}$, excellent agreement between theory and experiment is found. For the open circles, no corresponding FS could be assigned.

circles in Fig. 2). Alternatively, they might stem from fine structures of the branched FSs which hamper a further detailed analysis of these dHvA signals. Therefore, we will consider only well-defined FSs.

From the T dependence of the dHvA signal well above the critical field in the normal state, the effective cyclotron mass was calculated using the Lifshitz–Kosevich (LK) formula (Fig. 4, [31]). The dHvA results for different orientations together with the FPLO data are shown in Fig. 3 for three closed FSs. Since in the FPLO calculations no e-ph effects are included, the mass-enhancement factor, $\lambda = m_{\mathrm{exp}}/m_{\mathrm{FPLO}} - 1$, can be extracted directly from the experimental, m_{exp}, and theoretical, m_{FPLO}, effective masses. Renormalizations of nonphononic origin are expected to be weak. Point-contact measurements for the closely related system YNi_2B_2C [32] reveal a spectral density where all peaks can be assigned to well-known phonon modes. A weak nonphononic peak ($\lambda_P \approx 0.1$, likely a crystal-field excitation) has been detected only for the magnetic $HoNi_2B_2C$ [33]. In addition, if the coupling with antiferromagnetic spin fluctuations, e.g., caused by nesting effects, were strong, an unconventional, disorder-sensitive non-s-wave superconductivity would be expected, in conflict with the experimental data mentioned above. Thus, the band-resolved angular dependence of λ, shown in Fig. 3, is most likely directly related to the Cooper-pairing coupling parameter λ_{sc}. For all three bands, we find largely different coupling strengths and pronounced anisotropies, although there might be some remaining unresolved anisotropies due to the use of the quasiclassical LK analysis. The coupling of the spherical FS has a minimum along [001], with $\lambda \approx 0.3$, and a maximum along [110], $\lambda \approx 0.8$. Interestingly, the dHvA oscillations which belong to this FS are visible also below T_c, as long as the magnetic field is less than about 45° tilted away from the c axis [30]. In this range, we find a weak coupling of the electrons of $\lambda \leq 0.5$. Since the damping of the oscillations in the mixed-state is related to the opening of the superconducting gap, this observation suggests that these less strongly coupled electrons play a minor role in the superconductivity as already argued above.

For the "cushion"-like FS, $\lambda \approx 1$ in the (100) plane, but decreases continuously to about 0.25 towards [110]. This FS is supposed to be relevant for the coexistence of superconductivity and commensurate antiferromagnetism in the magnetic family members. Since the $5d$ states of the rare-earth atoms, which mediate the magnetic interaction between the localized rare-earth $4f$ magnetic moments, are not supposed to affect this FS, superconductivity may survive in this FS [34]. Recently, for $HoNi_2B_2C$ and $DyNi_2B_2C$, an averaged Eliashberg coupling constant $\lambda_{\mathrm{sc}} \approx 1$ was estimated in the context of point-contact

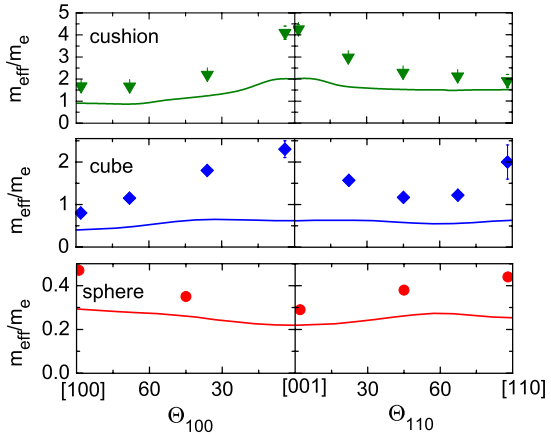

FIG. 3 (color online). Experimentally obtained effective masses of the cushion-, cubic-, and ball-like FSs (closed symbols). The solid lines represent the calculated effective masses.

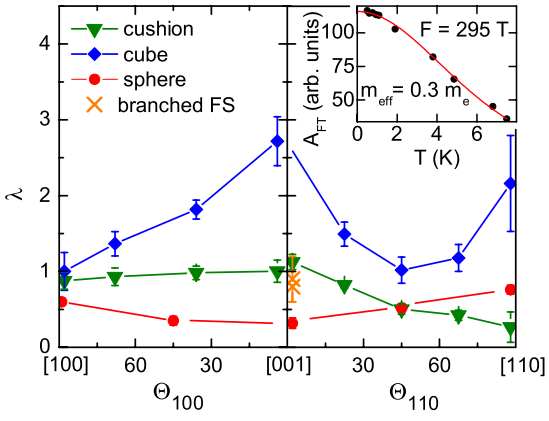

FIG. 4 (color online). Angular dependence of the mass-enhancement factor λ separated for three closed FSs and for the "branched" FS in one orientation. The inset shows the T dependence of the F_α frequency for a crystallographic orientation close to the [001] axis together with a LK fit.

tunneling data [33]. This is in good agreement with our results for the cushion sheet and supports the suggestion for the persisting superconductivity in this FS.

The ''cube''-like FS has a much stronger coupling with a maximum of $\lambda \approx 2.7$ along the [001] direction. λ is highly anisotropic reaching minima of about 1 along other directions. For the identified parts of the branched surface, we measured the effective masses along the [001] direction. We found values of $3.5m_e$ for the ''lemon'' and $3.6m_e$ for the ''windmill.'' From the comparison with the theoretically obtained bare masses, it follows that the coupling constant of the ''windmill'' is $\lambda = 0.8 \pm 0.2$ and that of the ''lemon'' is $\lambda = 0.9 \pm 0.3$. Thus, the coupling of both FSs is of intermediate strength for that orientation.

We may now compare our dHvA results with those of previous reports. Specific-heat data on polycrystalline samples point to $0.75 \leq \lambda_{sc} \leq 1.2$ [21,35,36]. High-temperature resistivity data, $\rho \propto \lambda_\rho T/\Omega_{pl}^2$, yield a transport coupling constant $\lambda_{tr} \approx 0.55$ to 1.1 [37]. Tunneling-spectroscopy data result in slightly lower λ_T values between 0.5 and 0.8 [10]. These experiments reveal information only about an averaged coupling strength. Therefore, a comparison with our data is not straight forward. However, averaging over all FSs our mean coupling constant agrees favorably well with these results.

In conclusion, we have presented theoretical and experimental band-structure investigations of the nonmagnetic borocarbide superconductor $LuNi_2B_2C$. By comparison of the effective masses obtained by dHvA measurements with calculated bare masses, the mass enhancement, or coupling strength, of different FSs has been extracted. Large anisotropies and differences in the absolute values of the coupling strengths were resolved indicating that the bands are differently involved in the formation of the superconducting state. This gives strong support for multiband superconductivity in $LuNi_2B_2C$ that has been suggested earlier [17–22] and provides new insight into the origin of the observed gap anisotropies [38].

The presented combination of highly sensitive dHvA measurements with precise electronic-structure calculations method provides a well-founded starting point for a detailed analysis of anisotropic multiband couplings in complex materials.

The work was supported by the DFG (SFB 463, SPP 1178, Emmy-Noether-program), EuroMagNET (No. RII3-CT-2004-506239), the EC program Transnational Access (No. RITA-CT-2003-505474), and at Ames Laboratory by the Department of Energy, Basic Energy Sciences (No. DE-AC02-07CH11358).

*Present address: Department of Phys., Techn. University of Denmark, 2800 Kongens Lyngby, Denmark

†Present address: Département de physique, Université de Montréal, Montréal, Québec H3C 3J7, Canada

[1] G. Grimval, *The Electron-Phonon Interaction in Metals* (North-Holland, Amsterdam, 1981).
[2] A. Carrington *et al.*, Phys. Rev. Lett. **91**, 037003 (2003); I. Mazin *et al.*, Phys. Rev. B **65**, 180510 (2002); H. Rosner *et al.*, *ibid.* **66**, 024521 (2002).
[3] K. Koepernik and H. Eschrig, Phys. Rev. B **59**, 1743 (1999).
[4] K. O. Cheon *et al.*, Physica C (Amsterdam) **312**, 35 (1999).
[5] G. W. Crabtree *et al.*, Phys. Rev. B **35**, 1728 (1987).
[6] R. J. Cava *et al.*, Nature (London) **367**, 252 (1994); R. Nagarajan *et al.*, Phys. Rev. Lett. **72**, 274 (1994).
[7] T. Ekino *et al.*, Physica C (Amsterdam) **235–240**, 2529 (1994).
[8] R. Movshovich *et al.*, Physica C (Amsterdam) **227**, 381 (1994).
[9] D. Lipp *et al.*, Europhys. Lett. **58**, 435 (2002).
[10] P. Martínez-Samper *et al.*, Phys. Rev. B **67**, 014526 (2003).
[11] T. Watanabe *et al.*, Phys. Rev. Lett. **92**, 147002 (2004).
[12] P. Raychaudhuri *et al.*, Phys. Rev. Lett. **93**, 156802 (2004).
[13] L. F. Mattheiss, Phys. Rev. B **49**, 13279 (1994).
[14] W. E. Pickett and D. J. Singh, Phys. Rev. Lett. **72**, 3702 (1994).
[15] H. Kim *et al.*, Phys. Rev. B **52**, 4592 (1995).
[16] S. B. Dugdale *et al.*, Phys. Rev. Lett. **83**, 4824 (1999).
[17] S. V. Shulga *et al.*, Phys. Rev. Lett. **80**, 1730 (1998).
[18] N. L. Bobrov *et al.*, Phys. Rev. B **71**, 014512 (2005).
[19] Y. G. Naidyuk *et al.*, Physica C (Amsterdam) **460–462**, 107 (2007).
[20] S. Mukhopadhyay *et al.*, Phys. Rev. B **72**, 014545 (2005).
[21] S. Manalo *et al.*, Phys. Rev. B **63**, 104508 (2001).
[22] T. Yokoya *et al.*, J. Phys. Chem. Solids **67**, 277 (2006).
[23] M. Xu *et al.*, Physica C (Amsterdam) **227**, 321 (1994).
[24] J. P. Perdew and Y. Wang, Phys. Rev. B **45**, 13244 (1992).
[25] W. Wong-Ng and R. S. Cava, Powder Diffr. **11**, 88 (1996).
[26] M. Tokunaga *et al.*, J. Phys. Soc. Jpn. **64**, 1458 (1995).
[27] K. Yamauchi *et al.*, Physica C (Amsterdam) **412–414**, 225 (2004).
[28] T. Terashima *et al.*, Solid State Commun. **96**, 459 (1995).
[29] L. H. Nguyen *et al.*, J. Low Temp. Phys. **105**, 1653 (1996).
[30] B. Bergk *et al.*, Physica C (Amsterdam) **460–462**, 630 (2007).
[31] D. Shoenberg, *Magnetic Oscillations in Metals* (Cambridge University Press, Cambridge, 1984).
[32] D. L. Baschlakov *et al.*, J. Low Temp. Phys. **147**, 335 (2007), Figs. 1–3.
[33] Yu. Naidyuk *et al.*, Phys. Rev. B **76**, 014520 (2007).
[34] S.-L. Drechsler *et al.*, Physica C (Amsterdam) **408–410**, 104 (2004).
[35] S.-L. Drechsler *et al.*, J. Low Temp. Phys. **117**, 1617 (1999).
[36] H. Michor *et al.*, Phys. Rev. B **52**, 16165 (1995).
[37] Using re-evaluated plasma frequency $\hbar\Omega_{pl} \approx 3.6(5.1)$ eV and a smaller single crystal value for $d\rho(T)/dT \approx 0.17(0.4)\ \mu\Omega\,\mathrm{cm/K}$ than in Ref. [14].
[38] Remaining underestimations of the gap anisotropies may be ascribed to anisotropies of other repulsive depairing interactions, e.g., density-wave fluctuations in the nesting directions [H. Kontani, Phys. Rev. B **70**, 054507 (2004).] or due to an anisotropic Coulomb interaction.